ADVANCED FUNCTIONAL MATERIALS
www.afm-journal.de

Controlled Assembly of MXene Nanosheets as an Electrode and Active Layer for High-Performance Electronic Skin

Xiyao Fu, Lili Wang, Lianjia Zhao, Zeyu Yuan, Yupu Zhang, Dongyi Wang, Depeng Wang, Junzhi Li, Dongdong Li, Valerii Shulga, Guozhen Shen,* and Wei Han**

MXenes are an emerging class of 2D transition metal carbides and nitrides. They have been widely used in flexible electronics owing to their excellent conductivity, mechanical flexibility, and water dispersibility. In this study, the electrode and active layer applications of MXene materials in electronic skins are realized. By utilizing vacuum filtration technology, few-layer MXene electrodes are integrated onto the top and bottom surfaces of the 3D polyacrylonitrile (PAN) network to form a stable electronic skin. The fabricated flexible device with $Ti_3C_2T_x$ MXene electrodes outperforms those with other electrodes and exhibits excellent device performance, with a high sensitivity of 104.0 kPa^{-1}, fast response/recovery time of 30/20 ms, and a low detection limit of 1.5 Pa. Furthermore, the electrode and the constructed MXene/PAN-based flexible pressure sensor exhibit robust mechanical stability and can survive 240 bending cycles. Such a robust, flexible device can be enlarged or folded like a jigsaw puzzle or origami and transformed from 2D to 3D structures; moreover, it can detect tiny movements of human muscles, such as movements corresponding to sound production and intense movements during bending of fingers.

1. Introduction

Electronic skins with high sensitivity, portability and foldability have gained significant attention for their use in artificial intelligence,[1–3] human-computer interaction,[4,5] health monitoring,[6,7] soft robotics, and disease detection.[8,9] A flexible pressure sensor is generally composed of a flexible substrate, an active layer, and a conductive electrode. The essential requirements of developing such a sensor are a considerable bending strain, high sensitivity, low driving voltage, fast response time, and excellent stability. The structure and morphology of the active layer are considered as key factors in improving the pressure-sensitive response of flexible devices.[10] The reported structures include interlocking microstructures,[11] hollow sphere microstructures,[12] lamellar structures,[13] porous structures,[14] and leaf impression.[15–17] In addition to the design of pressure-sensitive materials, a good electrode that covers the two opposite faces of the sensing film is also a critical component in determining the lifetime of flexible devices. Such electrodes must be compatible with the sensing thin film during the bending cycle and maintain their high electrical conductivity. Different electrode materials have been researched and are usually transformed into meshed networks or compact thin films. Indium tin oxide is the most widely used electrode material; however, its inherent brittleness hinders its potential application in wearable flexible electronic devices.[18] Ag nanowires have excellent electrical conductivity and are often used as electrode materials;[19] however, their functions are limited in practical applications. In addition, graphene materials are widely used because of their sufficient hydrophilicity and ability to easily form fairly uniform films on several substrates.[20,21] However, graphene film electrodes usually need to be transferred to a substrate through a complex process, which can introduce polymer impurities, and their conductivity needs to be improved.[22] To better adapt to the deformation of devices, a flexible electrode with high conductivity, which can be developed in a facile manner, is an indispensable component of next-generation flexible electronic devices.

MXenes, a family of 2D transition metal carbides and nitrides, are generally expressed by the formula $M_{n+1}X_nT_X$ ($n = 1$, 2, or 3), where M represents a transition metal (such as titanium,

X. Y. Fu, L. J. Zhao, Z. Y. Yuan, Y. P. Zhang, D. D. Li, V. Shulga, Prof. W. Han
Sino-Russian International Joint Laboratory for Clean Energy and Energy Conversion Technology
College of Physics & International Center of Future Science
Jilin University
Changchun 130012, P. R. China
E-mail: whan@jlu.edu.cn

Prof. L. L. Wang, D. P. Wang, Prof. G. Z. Shen
State Key Laboratory for Superlattices and Microstructures
Institute of Semiconductors
Chinese Academy of Sciences
Beijing 100083, P. R. China
E-mail: gzshen@semi.ac.cn

Prof. L. L. Wang, D. Y. Wang
State Key Laboratory on Integrated Optoelectronics
College of Electronic Science and Engineering
Jilin University
Changchun 130012, P. R. China
E-mail: lili_wang@jlu.edu.cn

Dr. J. Z. Li
Key Laboratory of Advanced Energy Materials Chemistry (Ministry of Education)
Renewable Energy Conversion and Storage Center
College of Chemistry
Nankai University
Tianjin 300071, P. R. China

The ORCID identification number(s) for the author(s) of this article can be found under https://doi.org/10.1002/adfm.202010533.

DOI: 10.1002/adfm.202010533

chromium, and vanadium), X is carbon and/or nitrogen, and T_X represents surface functional groups (hydroxyl, oxygen, or fluorine termination). They have been widely used in the fields of electromagnetic interference shielding,[23] solar cells,[24] catalysis,[25] and supercapacitors,[26] among others.[27,28] MXenes have also been proven to be a good choice for sensing materials due to their excellent electrical conductivity, rich chemicals, adjustable surface terminations, and controlled preparation process.[29,30] For example, Cheng et al. successfully fabricated an MXene-based pressure sensor with bioinspired microspinous microstructures through a printing process, which exhibited a high sensitivity of 151.4 kPa^{-1} and short response time of 130 ms.[31] In addition, a single-layer MXene has a high specific surface area and good surface hydrophilicity, which significantly enhances the force of binding with the contact substrate for better cyclic stability. Therefore, it is a good electrode material candidate for flexible devices.

In this work, we successfully fabricated a high-performance MXene/PAN composite film-based flexible pressure sensor with a uniform $Ti_3C_2T_x$ MXene electrode. This flexible device exhibits excellent pressure sensing performance and stability against mechanical bending. It also has a low detection limit of 1.5 Pa and a fast response time of 30 ms. This sensor offers a sensitivity that is ≈2–20 times higher than that of a similar sensor with traditional Ni, Cu, Au, or Ag electrodes. Moreover, we successfully detected the pulses, sound signals, and other human life activities using the fabricated MXene@PAN-based flexible pressure sensor, which confirmed its wide application prospects.

2. Results and Discussion

2.1. Material Synthesis and Device Fabrication

Figure 1a shows the overall fabrication process of the MXene-based flexible pressure sensor. First, a PAN precursor was electrospun onto aluminum foil using a nozzle (Figure S1a, Supporting Information), and then thermally dried at 60 °C for 4 h to connect the obtained PAN nanofibers, with an average diameter of 200 nm (Figure S1b, Supporting Information), to a 3D hierarchical planar network (Figure S1c, Supporting Information). Scanning electron microscope (SEM) images

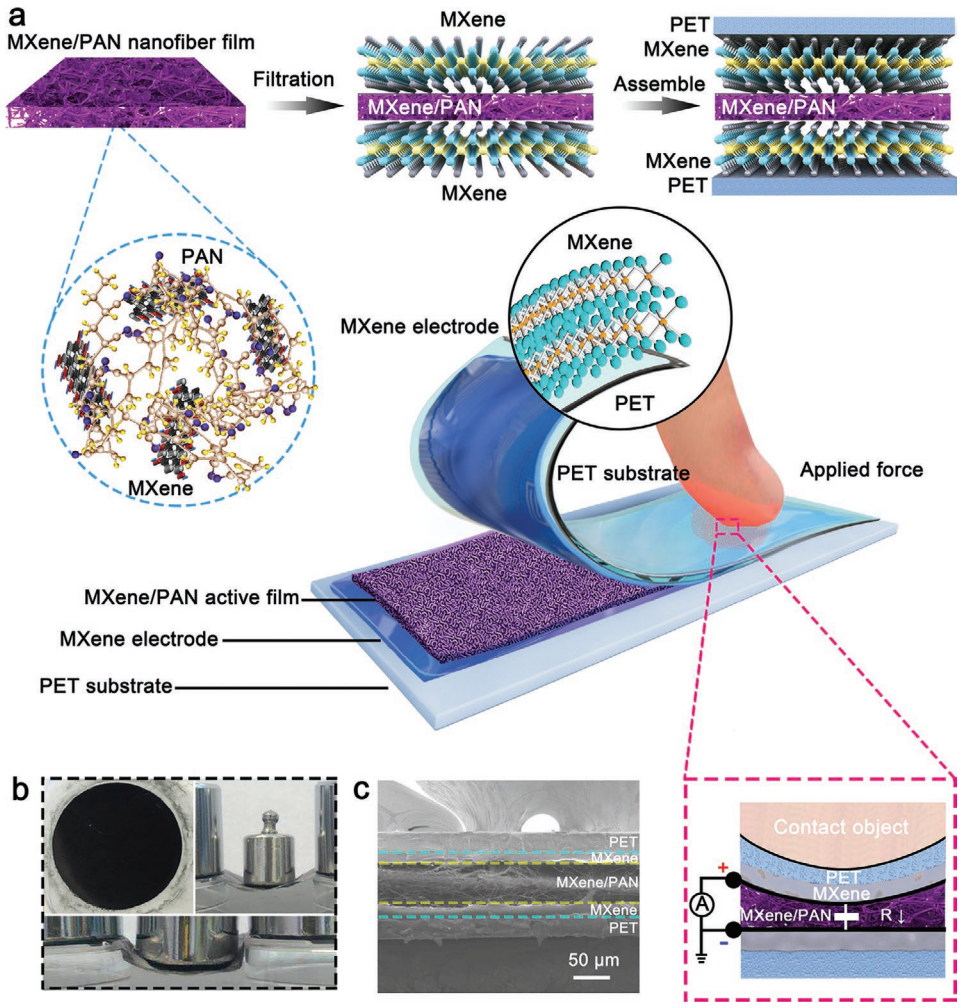

Figure 1. Device fabrication. a) The fabrication process for the MXene/PAN-based flexible pressure sensor with MXene electrode and working mechanism (inset). b) Optical image of the MXene/PAN thin film with MXene electrodes and their mechanical flexibility and strength. c) SEM image of the flexible pressure sensor with sandwich structure.

show that the PAN nanofibers are long enough to ensure that the nanowires can be crosslinked together to form a large open space in a 3D network structure for high deformation performance. For the top and bottom electrodes of the flexible pressure sensors, MXene thin films were successively deposited on the top and bottom surfaces of the electrospun PAN 3D porous networks using vacuum filtration. This process allows the MXene nanosheets to penetrate the PAN 3D network, enhances the conductivity of PAN, and improves the binding force of MXene as an electrode and sensitive film, thus improving the stability of the device. Figure 1a illustrates the concept and structure of the pressure-sensitive electronic skin that consists of a flexible PET substrate, thin MXene ($Ti_3C_2T_X$) film electrodes (Figure S2, Supporting Information), and a composite film. The MXene/PAN 3D porous film is used as the pressure-sensitive layer. Figure 1b shows that the MXene/PAN conductive film with an MXene electrode prepared by vacuum filtration has good mechanical stability and strong flexibility. Figure 1c shows a cross-sectional SEM image of the flexible pressure sensor with a sandwich structure (PET/MXene/MXene/PAN/MXene/PET). These designs help to minimize bending-induced strains. The compression mechanism is illustrated in Figure 1a. When pressure was applied, the interstice of the fiber network was compressed, making the MXene nanosheets come into closer contact with each other. Owing to the excellent conductivity of MXenes, the close contact of more MXene nanosheets increased the number of current pathways, which in turn significantly increased the contact area of the composite fiber network. When the pressure was removed, the 3D porous network quickly returned to its original fluffy state because of the excellent flexibility of the nanofibers.

2.2. Material Characterization

Figure 2a,b depicts the MXene nanosheets interspersed between the fibers, forming a unique 3D fiber network structure. The successful fabrication of the MXene/PAN composite nanofiber film was also confirmed by X-ray powder diffraction (XRD), energy-dispersive spectroscopy (EDS), and Fourier transform infrared spectroscopy (FTIR). The XRD pattern in Figure 2c shows that the peaks of the MXene/PAN composite film confirmed the existence of two substances. The characteristic peak of $Ti_3C_2T_x$ located at 2θ of 6.86° represents the diffraction from the (002) surface of $Ti_3C_2T_x$. The prominent peak at 2θ of ≈17° represents the characteristic peak of PAN materials.[32] Elemental mapping analyses revealed that Ti, C, O, N, and F elements were distributed in the position of each layer of the device (Figure 2d). The FTIR spectra of the MXene/PAN film (Figure 2e) exhibited absorption peaks corresponding to stretching vibrations at 2923 cm^{-1} (C–H), 2241 cm^{-1} (C≡N), 1728 cm^{-1} (C=O), and 1450 cm^{-1} (C–H). These results were consistent with those of the PAN spectra, proving the successful fabrication of the composite film.[33] The existence of MXene nanosheets in the composite film was further explored through Raman spectroscopy (Figure S3, Supporting Information). The adsorption peaks at ≈207 and 722 cm^{-1} were attributed to the Ti–C and C–C vibrations of the oxygen-terminated

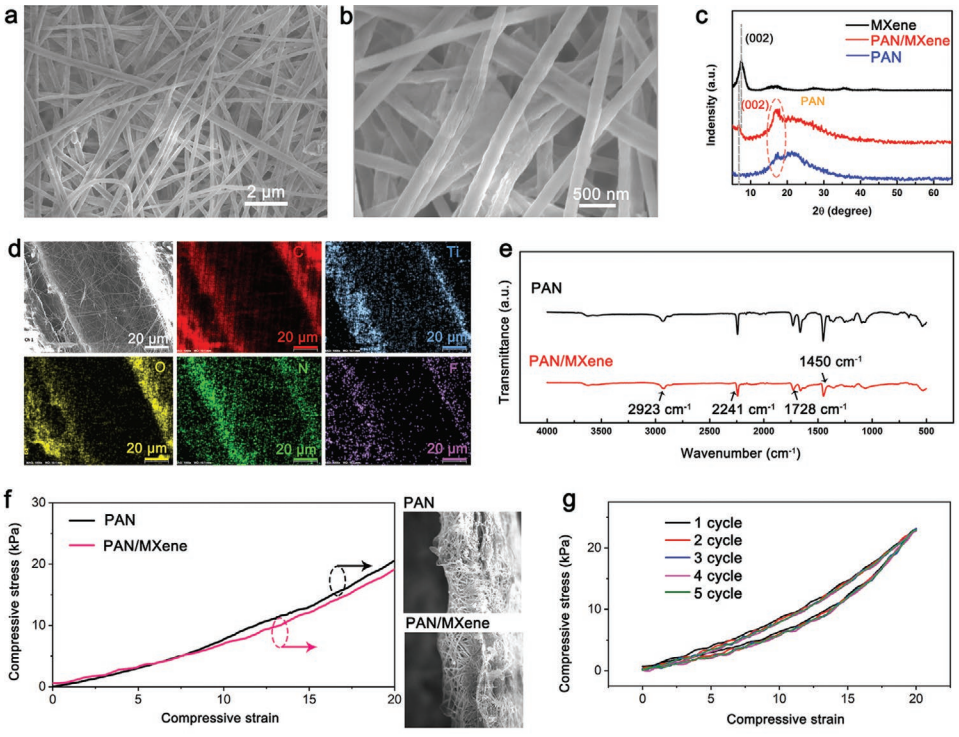

Figure 2. Material characterization. a,b) SEM image of MXene/PAN composite film with 3D porous structure. c) XRD patterns of pristine MXene, PAN, and MXene/PAN samples. d) EDS mapping of the MXene/PAN composite film with MXene electrodes. e) FTIR spectra of the pristine PAN and MXene/PAN film. f) Typical compression stress–strain curves of pristine PAN film and MXene/PAN composite film. Inset show the SEM image of pristine PAN and MXene/PAN composite film. g) Five consecutive compression tests on the MXene/PAN composite nanofiber film.

$Ti_3C_2T_X$ MXene, respectively. The peaks at 388 and 571 cm^{-1} can be assigned to the vibrations of O atoms (E_g and A_{1g}, respectively).[34] The above analysis results were consistent with the XRD results. The typical compression stress–strain curves of the pristine PAN film and MXene/PAN composite film are shown in Figure 2f. The compressive elastic modulus and stress at 20% strain of the MXene/PAN composite film were calculated as 0.87 MPa and 22.5 kPa, respectively. The elastic modulus and stress of the pristine PAN film (0.98 MPa and 23.7 kPa, respectively) have no evident fluctuation, indicating that the introduction of MXene did not damage the 3D PAN porous structure (Figure 2f) and mechanical properties. Hysteresis in the mechanical and electrical performance is quantified as the maximum difference between the load and unload curves divided by the full-size output. The hysteresis rate of the MXene/PAN composite film at the maximum sensitivity of 22 kPa is 7.9% (Figure 2g), which is much lower than the hysteresis rate of the conductive foam. The hysteresis phenomenon is reduced under low strain, which proves the effectiveness of the sensor in a low-pressure environment.

2.3. Pressure-Sensitive Properties

To examine the sensing performance of the MXene/PAN-based flexible pressure sensor with MXene electrodes, other electrode-based MXene/PAN-based flexible pressure sensors were fabricated using the same technology. **Figure 3**a presents a comparison of the pressure-sensitive response of the proposed sensors with that of a device with identical structure but different electrodes at 4 kPa. MXene-based devices exhibit higher pressure sensitivity than devices based on other electrodes,

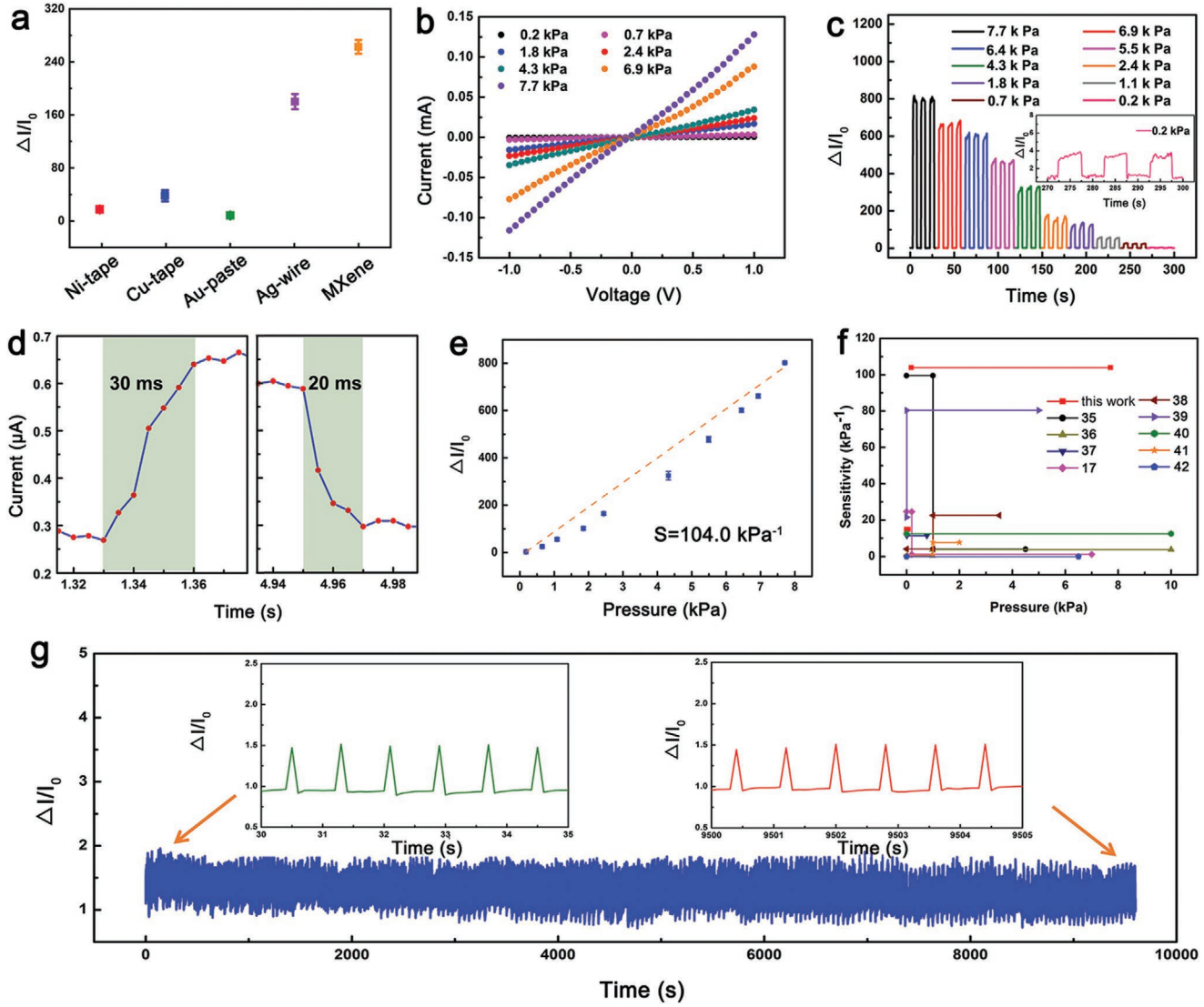

Figure 3. Sensing properties of MXene/PAN film-based flexible sensors. a) Pressure sensitive response of the flexible sensor with different electrodes at 4 kPa. b) Current change of MXene/PAN film-based sensor under applied pressure ranging from 0.2 to 7.7 kPa. c) Corresponding dynamic response/recovery behaviors. d) Response and recovery time of the flexible sensor. e) Ultrahigh linear sensitivity of the sensor under pressure from 0.2 to 7.7 kPa ($n = 3$ measurements). f) Summary of pressure sensitive performance of MXene-based flexible pressure sensor. g) Durability performance of flexible sensor after 10 000 cycling tests at 0.2 kPa.

such as those of Ni-tape, Cu-tape, Au-paste, and Ag-wire. Figure 3b presents the current–voltage (I–V) curves of the flexible film as functions of pressure. When the pressure increased from 0.2 to 7.7 kPa, the change in current increased. This finding indicated that the sensor can distinguish different pressures over a wide range. Dynamic pressure-sensitive response curves over the same pressure range (Figure 3c) also demonstrated good response/recovery behaviors. The response and recovery times of the flexible sensor were 30 and 20 ms, respectively (Figure 3d and Figure S4: Supporting Information), which are less than those of the other MXene-based pressure sensors.[30,31] The sensitivity calculated by the ratio of the slope of the change-in-current to the change-in-pressure is represented as $S = \delta(\Delta I/I_0)/\delta p$, where $\Delta I = I - I_0$, I is the current under loading, I_0 is the current without loading, and p is the pressure applied on the sensor. The sensitivity is an important parameter for evaluating the performance of a pressure sensor. By fitting the curve in Figure 3e, sensitivity was 104.0 kPa^{-1} on a pressure scale from 0.2 to 7.7 kPa. The sensitivity of our sensor is higher than that of the pristine MXene film (Figure S5, Supporting Information) and the previously reported MXene-based sensor (Figure 3f) and Table S1 (Supporting Information).[17,35–43] We further attempted to monitor the sensor in a lower pressure range. As shown in Figure S6a (Supporting Information), the flexible sensor creates accurate differentiation for different pressures within the pressure range of 0–61 Pa, and a good linear relationship is maintained for the I–V curves. Meanwhile, the detection limit of the MXene/PAN-based flexible pressure sensor was as low as 1.5 Pa (Figure S6b, Supporting Information). For flexible pressure-sensitive devices, high mechanical durability under long-time or cyclic use also plays an important role in the reliable input-output relation. Repeated compression/release tests over 10 000 cycles were performed at a peak pressure of ≈0.2 kPa, and no signal drift or fluctuation was observed in the cyclic test (Figure 3g). A comparison of the previous cycle and the following five cycles (Figure 3g) shows that the value and shape of the peaks for the electrical signals were almost unchanged, which indicated that the sensor had excellent cyclic stability and long working life. To determine the stability of the sensor, the pressure-sensitive signal of the sensor has no obvious change after several days in the air, which proves that the sensor has good long-term stability (Figure S7, Supporting Information).

2.4. Mechanical Properties and Human Physiological Activities

The mechanical properties of flexible sensors should also be considered in medical devices.[44,45] **Figure 4**a shows the variation in the flexible sensor's current at different bending angles.

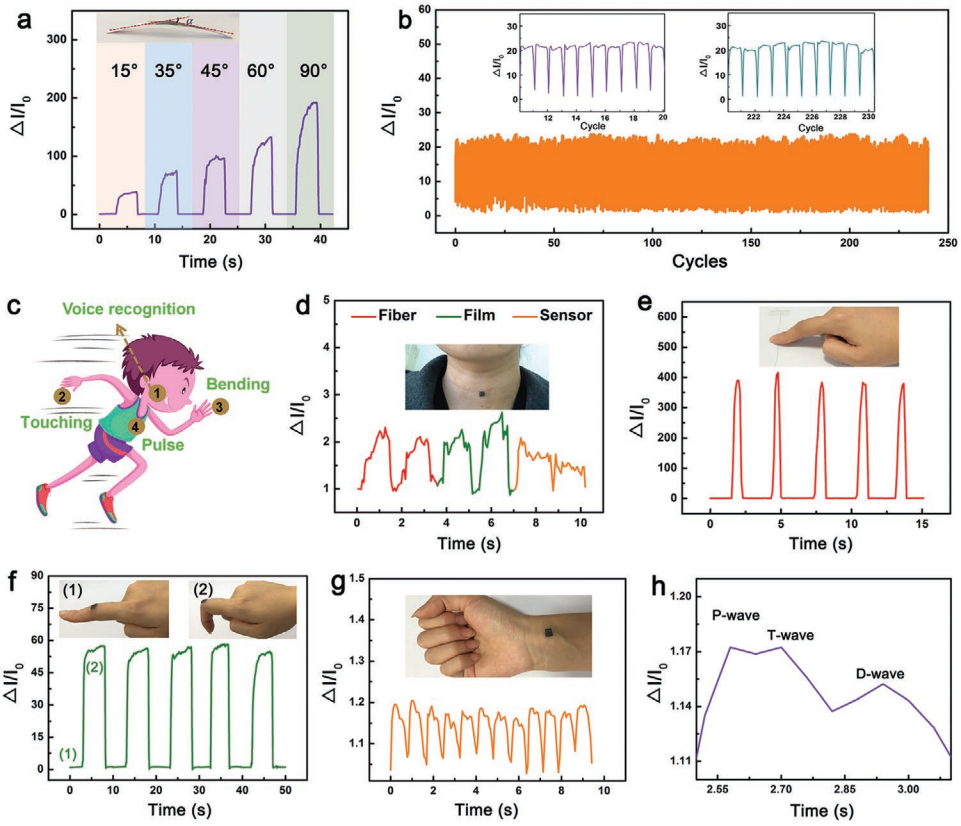

Figure 4. Real-time detecting human physiological activities. a) Dynamic response curves of flexible pressure sensor under different bending angles. b) Bending responses over 240 cycles at a bending angle of ≈15°. c) Illustration of human physiological activities. d) Relative current change of MXene/PAN flexible sensor under different sound stimuli, for instance "fiber", "film", and "sensor". e) Responsive curves while finger was pressed on the pressure sensor. f) Sensing performance of the pressure sensor attached to the finger for continuous detection of finger bending training. g) Response to the monitoring of wrist pulse. h) The enlarged waveform of the blood pulse.

The current change was positively correlated with the increase in the bending angle from 15° to 90°. Figure 4b suggests that the flexible pressure sensor maintains significant mechanical robustness with no evident fatigue after 240 bending/unbending cycles at a bending angle of ≈15°. The high reliability under cyclic bending indicates that this pressure device is a promising tool for the detection of bending-related motions. To demonstrate the potential of the MXene@PAN-based flexible pressure sensor as a wearable device, we used an assembled sensor to monitor human physiological activities, such as voice recognition, touching, bending, and pulsation (Figure 4c).

As shown in Figure 4d, the MXene/PAN-based flexible pressure sensor was attached to the subject's throat to detect the movement of tiny muscles during vocalization. The pressure sensor produced distinct patterns in the vocalization of different words, such as "good morning" (Figure S8, Supporting Information), "fiber", "film", and "sensor", suggesting the potential application of the sensor in artificial intelligence and voice assistance. The pressure sensor also exhibited clear and steady signals, regardless of whether the finger moved quickly (Figure 4e) or slowly (Figure S9, Supporting Information). Furthermore, we applied the MXene/PAN-based flexible pressure sensor to monitor the flexion/extension of the human finger, and the sensor displayed a higher sensitivity while the finger was bent (Figure 4f). Meanwhile, the device can monitor articular nimbleness by continuous bending of the finger to different angles (Figure S10, Supporting Information). Pulse waves can provide significant data on heart conditions and heart-related diseases. Thus, we attached the pressure sensor to the wrist and neck of a 26-year-old female. The analysis of stationary signals, as presented in Figure 4g and Figure S11 (Supporting Information), shows radial and carotid artery frequencies of 72 pulses min^{-1}, indicating that the person has good health. The characteristic peaks of the pulse (P-wave, T-wave, and D-wave corresponding to percussion wave, tidal wave, and diastolic pressure, respectively) were clearly captured and distinguished, which proved that the $Ti_3C_2T_X$/PAN sensor can provide support for health monitoring and disease surveillance.

2.5. Applications and Displays of Flexible Sensors

In addition to the above features, the MXene/PAN-based flexible sensor has good conformability to various arbitrary surfaces and can be transformed from a 2D to 3D structure. The MXene/PAN film was attached to the fixed area of the six alternative layers of origami as response indicators (**Figure 5**a,b). Then, we applied layer-relevant resistance changes in parallel with a one-sided origami hierarchical sensor array at 0.5 kPa (Figure S12, Supporting Information). The results showed that the pressure-sensitive response did not change significantly, indicating that different unit devices have uniformity properties. We further evaluated the reproducibility of each device. The results showed that the pressure-sensitive characteristics of a single origami layered sensor array have robust reproducibility (Figure 5c and Video S1: Supporting Information). The in-plane 2D pressure sensor array was then transformed into an integrated folding device (Figure 5d) by folding it to form a one-sided hierarchical sensor array following the origami method and then pressing it for 20 min. This design is compact, thus making the device suitable for special applications, such as those in badminton courts without judges; such a design also improves the diversity and portability of wearable electronic devices. The response of the layer-by-layer pressure is similar to that of the origami hierarchical sensor array because of the similarity of the laminated structure. Thus, when the same pressure is applied, the pressure-sensitive response of the integrated folding device rapidly reaches the maximum value because of the simultaneous deformation of multiple array devices (Figure 5e and Video S2: Supporting Information). Furthermore, the sharp peaks in Figure 5f reflect the high-frequency tapping of the index finger, thus indicating that the sensor array is more sensitive than a single pressure sensor. In addition, bending and straightening cycles of the human wrist (Figure 5g) and elbow (Figure 5h) were performed. The sharp on/off peaks clearly display the fast response and high sensitivity of the integrated folding device, whereas the peak intensity of each separate curve remains relatively stable during the same motion process.

A simple circuit diagram was designed to further verify the satisfactory response of the $Ti_3C_2T_X$/PAN sensor over a wide range, as shown in Figure 5i. Under an external power supply of 3 V, the pressure sensor and LED were connected in series to form a closed loop. The prepared sensor was equivalent to a rheostat. The resistance of the sensor changed when different pressures were received, and the voltage at both ends of the LED changed correspondingly. This condition was visually represented by the change in the brightness of the LED. The applied pressures were 4.90, 1.96, 0.98, 0.49, 0.19, and 0.10 kPa as the LED output changed from bright to dim (Figure 5j). This finding demonstrated that the sensor resistance decreased with the increase in applied pressure; this feature can be applied to the load monitoring of bridges and roads. For instance, when the vehicle load exceeds a certain limit, the light alarm will be turned on.

3. Conclusion

In summary, we developed an MXene/PAN-based flexible pressure sensor with MXene electrodes. The flexible pressure sensor not only significantly improves pressure-sensitive responses as compared with sensors based on other electrodes, but also exhibits good cyclic stability (over 10 000 cycles), fast response time, low detection limit, and high stability. The fabricated flexible $Ti_3C_2T_X$/PAN composite film can be used as a pressure sensor to accurately and rapidly monitor human physiological activities, making it suitable for applications such as voice recognition and pulse monitoring, owing to its fast response and high stability. The high performance of the MXene/PAN-based flexible pressure sensor, as demonstrated in this study, highlights its great potential for application in intelligent flexible systems, including soft robots, bionic robots, tactile feedback systems, and biomedical equipment. Furthermore, an origami-inspired folding device consumes less space, thus making it suitable for special applications: such a compact design improves diversity and portability of wearable electronic devices. This study provides a new application prospect for MXenes and polymer fiber composite structures as sensing materials to improve the sensing performance and mechanical property of wearable electronic devices.

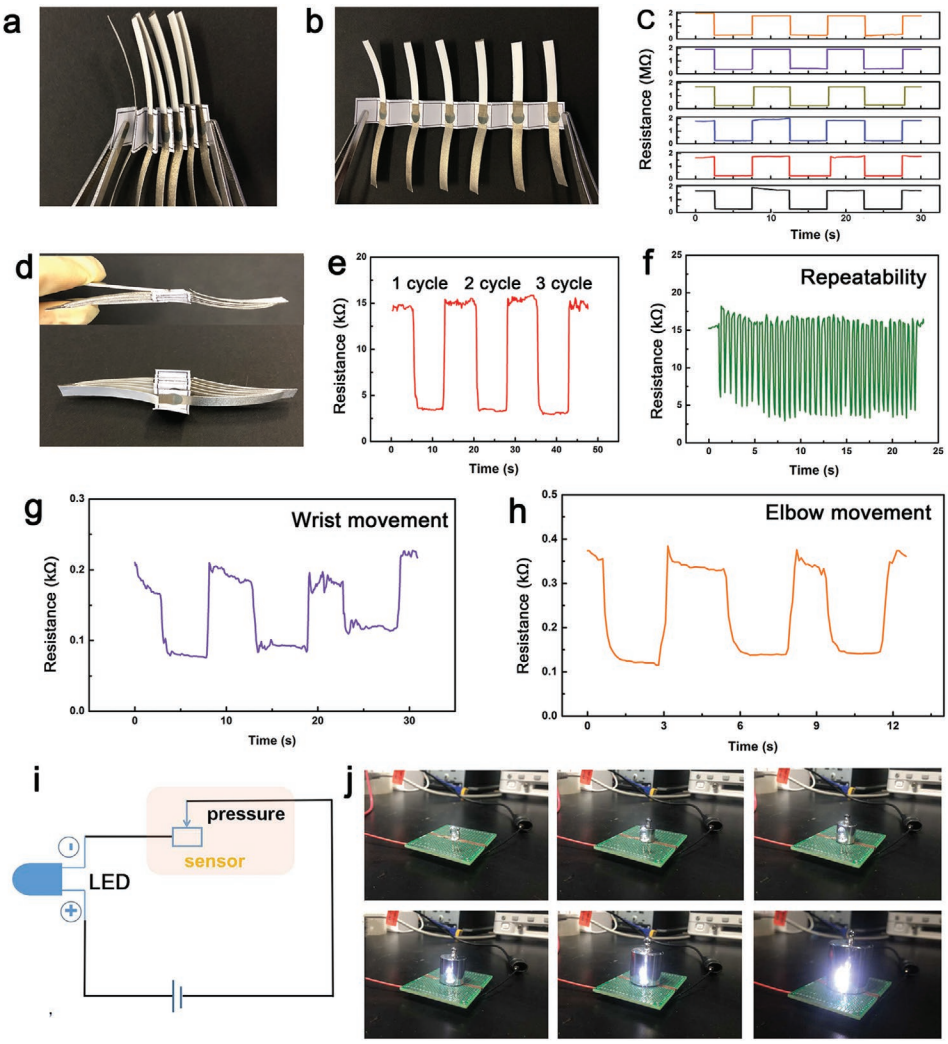

Figure 5. Applications and displays of MXene/PAN-based flexible pressure sensors. a,b,d) Images describing the design of six-channel pressure sensor integrated on a folding paper. Real-time monitoring of the resistance change for c) a single device and e) integrated folding device during continuous loading and unloading processes. f) Repeatability performance of the integrated folding device under continuous loading-unloading cycles. Real-time recorded resistance changes of bending-releasing movements of the g) wrist and h) elbow. i) Circuit diagram of $Ti_3C_2T_X$/PAN sensor and LED. j) The brightness response of LED varied with different applied pressure on the MXene/PAN flexible sensors.

4. Experimental Section

Synthesis of Few-Layer MXenes ($Ti_3C_2T_x$): 1.5 g of Ti_3AlC_2 powder was slowly added to a 30 mL of an acidic solution, where the volume ratio of deionized (DI) water, hydrochloric acid (12 M), and hydrofluoric acid (49%) was 4.5: 4.5: 1. After stirring at room temperature for 24 h, it was taken out and washed repeatedly with deionized water until the pH value was neutral. The as-obtained multi-layer $Ti_3C_2T_x$ was transferred to a LiCl solution, which was stirred for 4 h for intercalation. Afterward, the mixture was washed with deionized water via centrifugation (5 min per cycle at 6000 rpm), followed by ultrasound imaging for 2 h. The resulting few-layer $Ti_3C_2T_x$ solution had a measured concentration of 2 mg mL^{-1}.

Preparation of PAN Fiber Membrane: PAN powder was dissolved in *N*,*N*-dimethylformamide (DMF) solvent and prepared as a precursor solution with a mass fraction of 8%. The solution was stirred at room temperature for 5 h. Electrospinning was performed at a flow rate of 1 mL h^{-1} with applied voltage 19 kV. The aluminum foil on the stainless-steel substrate serves as the receiving base of the electrospinning fiber film. Keep the collector at a distance of 12 cm from the syringe. The obtained product was dried in the oven for 1 h at 60 °C.

Preparation of MXene/PAN Film: Cut the dry PAN fiber membrane into a circle with a diameter of 4 cm as the base material. 5 mL prepared MXene solution was vacuum filtered through PAN film. When all the solution permeated through the membrane, vacuum was disconnected immediately. Then transfer $Ti_3C_2T_X$/PAN film to vacuum drying oven for 6 h at room temperature. As a control, a pure MXene membrane obtained by filtration was prepared.

Characterization: The surface morphology of the prepared composite membrane were captured by scanning electron microscopy (SEM, Magellan 400). X-ray diffractometer (XRD, Rigak D/max 2550 V) and FTIR spectrometer (Nicolet IS10) were used for identifying material components. To collect changes in the electrical signal of the pressure sensor, CHI760E Electrochemical workstation (CH Instruments Inc., Shanghai, China) was required.

Supporting Information

Supporting Information is available from the Wiley Online Library or from the author.

Acknowledgements

The authors thank the authors sincerely acknowledge financial support from the National Natural Science Foundation of China (NSFC Grant No. 61874111, 61625404, 21571080, 61888102, 21903034), the Science and Technology Development Plan of Jilin Province (20190103135JH), Young Elite Scientists Sponsorship Program by CAST (2018QNRC001) and Foshan Innovative and Entrepreneurial Research Team Program (No. 2018IT100031). Informed consent was obtained form all volunteers who participated in this study.

Conflict of Interest

The authors declare no conflict of interest.

Data Availability Statement

Research data are not shared.

Keywords

3D MXene/PAN networks, flexible pressure sensors, high sensitivity, MXene electrodes, robust structures

Received: December 7, 2020
Revised: January 8, 2021
Published online:

[1] L. Wang, D. Chen, K. Jiang, G. Shen, *Chem. Soc. Rev.* **2017**, *46*, 6764.
[2] S. Lee, A. Reuveny, J. Reeder, S. Lee, H. Jin, Q. Liu, T. Yokota, T. Sekitani, T. Isoyama, Y. Abe, Z. Suo, T. Someya, *Nat. Nanotechnol.* **2016**, *11*, 472.
[3] X. Tang, C. Wu, L. Gan, T. Zhang, T. Zhou, J. Huang, H. Wang, C. Xie, D. Zeng, *Small* **2019**, *15*, 1804559.
[4] Q. Liu, Z. Liu, C. Li, K. Xie, P. Zhu, B. Shao, J. Zhang, J. Yang, J. Zhang, Q. Wang, C. F. Guo, *Adv. Sci.* **2020**, *7*, 2000348.
[5] R. Zhang, M. Hummelgård, J. Örtegren, Y. Yang, H. Andersson, E. Balliu, N. Blomquist, M. Engholm, M. Olsen, Z. L. Wang, H. Olin, *Nano Energy* **2019**, *63*, 103842.
[6] L. L. Wang, Z. Lou, K. Wang, S. F. Zhao, P. C. Yu, W. Wei, D. Y. Wang, W. Han, K. Jiang, G. Z. Shen, *Research* **2020**, *2020*, 8716847.
[7] Y. Lin, M. Bariya, H. Y. Y. Nyein, L. Kivimäki, S. Uusitalo, E. Jansson, W. Ji, Z. Yuan, T. Happonen, C. Liedert, J. Hiltunen, Z. Fan, A. Javey, *Adv. Funct. Mater.* **2019**, *29*, 1902521.
[8] Z. Liu, Z. Zhao, X. Zeng, X. Fu, Y. Hu, *Nano Energy* **2019**, *59*, 295.
[9] Y. Gao, H. Ota, E. W. Schaler, K. Chen, A. Zhao, W. Gao, H. M. Fahad, Y. Leng, A. Zheng, F. Xiong, C. Zhang, L. C. Tai, P. Zhao, R. S. Fearing, A. Javey, *Adv. Mater.* **2017**, *29*, 1701985.
[10] P. Sriram, A. Manikandan, F. Chuang, Y. Chueh, *Small* **2020**, *16*, 1904271.
[11] C. Zhang, W. B. Ye, K. Zhou, H. Y. Chen, J. Q. Yang, G. Ding, X. Chen, Y. Zhou, L. Zhou, F. Li, S. T. Han, *Adv. Funct. Mater.* **2019**, *29*, 1808783.
[12] L. Wang, X. Huang, D. Wang, W. Zhang, S. Gao, J. Luo, Z. Guo, H. Xue, J. Gao, *Chem. Eng. J.* **2021**, *405*, 127025.
[13] Z. Sang, K. Ke, I. Manas-Zloczower, *Small* **2019**, *15*, 1903487.
[14] D. Y. Wang, L. L. Wang, Z. Lou, Y. Q. Zheng, K. Wang, L. J. Zhao, W. Han, K. Jiang, G. Z. Shen, *Nano Energy* **2020**, *78*, 105252.
[15] Z. Ma, D. Kong, L. J. Pan, Z. N. Bao, *J. Semicond.* **2020**, *41*, 041601.
[16] H. B. Yao, J. Ge, C. F. Wang, X. Wang, W. Hu, Z. J. Zheng, Y. Ni, S. H. Yu, *Adv. Mater.* **2013**, *25*, 6692.
[17] D. Y. Wang, L. Wang, G. Shen, *J. Semicond.* **2020**, *41*, 041605.
[18] S. Leung, K. Ho, P. Kung, H. A. V. Hsiao, Z. Wang, J. He, *Adv. Mater.* **2018**, *30*, 1704611.
[19] L. L. Wang, S. Chen, W. Li, K. Wang, Z. Lou, G. Z. Shen, *Adv. Mater.* **2019**, *31*, 1804583.
[20] W. S. Lee, D. Kim, B. Park, H. Joh, H. K. Woo, Y.-K. Hong, T.-i. Kim, D.-H. Ha, S. J. Oh, *Adv. Funct. Mater.* **2019**, *29*, 1806714.
[21] A. AlAmri, S. Leung, M. Vaseem, A. Shamim, J. He, *IEEE Trans. Electron Devices* **2019**, *66*, 2657.
[22] K. Yong, S. De, E. Y. Hsieh, J. Leem, N. R. Aluru, S. Nam, *Mater. Today* **2020**, *34*, 58.
[23] M. Han, C. E. Shuck, R. Rakhmanov, D. Parchment, B. Anasori, C. M. Koo, G. Friedman, Y. Gogotsi, *ACS Nano* **2020**, *14*, 5008.
[24] L. Yang, Y. Dall'Agnese, K. Hantanasirisakul, C. E. Shuck, K. Maleski, A. Mohamed, G. Chen, Y. Gao, Y. Sanehira, A. K. Jena, L. Shen, C. Dall'Agnese, X.-F. Wang, Y. Gogotsi, T. Miyasaka, *J. Mater. Chem. A* **2019**, *7*, 5635.
[25] Z. Li, Y. Wu, *Small* **2019**, *15*, 1804736.
[26] S. Xu, G. Wei, J. Li, W. Han, Y. Gogotsi, *J. Mater. Chem. A* **2017**, *5*, 17442.
[27] J. L. Zhao, K. Wang, W. Wei, L. L. Wang, W. Han, *InfoMat* **2019**, *1*, 407.
[28] J. X. Nan, X. Guo, J. Xiao, X. Li, W. Chen, W. Wu, H. Liu, Y. Wang, M. Wu, G. Wang, *Small* **2019**, 1902085.
[29] K. Wang, Z. Lou, L. Wang, L. Zhao, S. Zhao, D. Wang, W. Han, K. Jiang, G. Shen, *ACS Nano* **2019**, *13*, 9139.
[30] Y. Ma, N. Liu, L. Li, X. Hu, Z. Zou, J. Wang, S. Luo, Y. Gao, *Nat. Commun.* **2017**, *8*, 1207.
[31] Y. Cheng, Y. Ma, L. Li, M. Zhu, Y. Yue, W. Liu, L. Wang, S. Jia, C. Li, T. Qi, J. Wang, Y. Gao, *ACS Nano* **2020**, *14*, 2145.
[32] M. Naraghi, S. N. Arshad, I. Chasiotis, *Polymer* **2011**, *52*, 1612.
[33] J. A. Wahab, P. K. Gianchandani, I. S. Kim, Q. Q. Ni, *Ultrason. Sonochem.* **2019**, *51*, 399.
[34] A. Sarycheva, T. Makaryan, K. Maleski, E. Satheeshkumar, A. Melikyan, H. Minassian, M. Yoshimura, Y. Gogotsi, *J. Phys. Chem. C* **2017**, *121*, 19983.
[35] Y. Gao, C. Yan, H. Huang, T. Yang, G. Tian, D. Xiong, N. Chen, X. Chu, S. Zhong, W. Deng, Y. Fang, W. Yang, *Adv. Funct. Mater.* **2020**, *30*, 1909603.
[36] Y. Guo, M. Zhong, Z. Fang, P. Wan, G. Yu, *Nano Lett.* **2019**, *19*, 1143.
[37] Y. Zhang, T. H. Chang, L. Jing, K. Li, H. Yang, P. Y. Chen, *ACS Appl. Mater. Interfaces* **2020**, *12*, 8392.
[38] Y. Ma, Y. Yue, H. Zhang, F. Cheng, W. Zhao, J. Rao, S. Luo, J. Wang, X. Jiang, Z. Liu, N. Liu, Y. Gao, *ACS Nano* **2018**, *12*, 3209.
[39] Y. Hu, H. Zhuo, Q. Luo, Y. Wu, R. Wen, Z. Chen, L. Liu, L. Zhong, X. Peng, R. Sun, *J. Mater. Chem. A* **2019**, *7*, 10273.
[40] Z. Chen, Y. Hu, H. Zhuo, L. Liu, S. Jing, L. Zhong, X. Peng, R.-c. Sun, *Chem. Mater.* **2019**, *31*, 3301.
[41] R. Liu, J. Li, M. Li, Q. Zhang, G. Shi, Y. Li, C. Hou, H. Wang, *ACS Appl. Mater. Interfaces* **2020**, *12*, 46446.
[42] X. P. Li, Y. Li, X. Li, D. Song, P. Min, C. Hu, H. B. Zhang, N. Koratkar, Z. Z. Yu, *J. Colloid Interface Sci.* **2019**, *542*, 54.
[43] R. Qin, M. Hu, X. Li, L. Yan, C. Wu, J. Liu, H. Gao, G. Shan, W. Huang, *Nanoscale* **2020**, *12*, 17715.
[44] H. Medina, J. Li, T. Su, Y. Lan, S. Lee, C. Chen, Y. Chen, A. Manikandan, S. Tsai, A. Navabi, X. Zhu, Y. Shih, W. Lin, J. Yang, S. Thomas, B. Wu, C. Shen, J. Shieh, H. Lin, A. Javey, K. Wang, Y. Chueh, *Chem. Mater.* **2017**, *29*, 1587.
[45] Y. Chen, Y. You, P. Chen, D. Li, T. Su, L. Lee, Y. Shih, C. Chen, C. Chang, Y. Wang, C. Hong, T. Wei, J. Ho, K. Wei, C. Shen, Y. Chueh, *ACS Appl. Mater. Interfaces* **2018**, *10*, 35477.